

AD-A070 479

MARYLAND UNIV COLLEGE PARK DEPT OF PHYSICS AND ASTRONOMY F/G 20/9  
INFLUENCE OF STRONG SELF ELECTRIC FIELDS ON THE ION RESONANCE I--ETC(U)  
1977 R C DAVIDSON  
PUB-77-226

N00014-75-C-0309

NL

UNCLASSIFIED

| OF |  
AD  
A070 479



END  
DATE  
FILMED  
8-79  
DDC

Code 8702

ADA070479

PREPRINT 705P002

INFLUENCE OF STRONG SELF ELECTRIC FIELDS ON THE ION RESONANCE INSTABILITY  
IN A NONNEUTRAL PLASMA COLUMN

Ronald C. Davidson  
Division of Magnetic Fusion Energy  
Energy Research and Development Administration  
Washington, D. C. 20545

Hwan-sup Uhm  
Department of Physics and Astronomy  
University of Maryland, College Park, Md. 20742

Physics Publication Number 77-226

1977

APPROVED FOR PUBLIC RELEASE  
DISTRIBUTION UNLIMITED

Work on this report was supported  
by ONR Contract N00014-75-C-0309  
and/or N00014-67-A-0239  
monitored by NRL 6702.  
02.



UNIVERSITY OF MARYLAND  
DEPARTMENT OF PHYSICS AND ASTRONOMY  
COLLEGE PARK, MARYLAND

79 06 22 815

ADA070479

DDC ACCESSION NUMBER

**II**  
LEVEL

DDC PROCESSING DATA

PHOTOGRAPH

THIS SHEET

RETURN TO DDA-2 FOR FILE

**I**  
INVENTORY

Preprint 705P002, Physics Pub. 77-226

DOCUMENT IDENTIFICATION

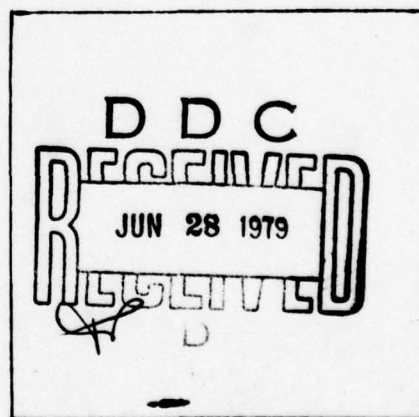
**DISTRIBUTION STATEMENT A**

Approved for public release;  
Distribution Unlimited

DISTRIBUTION STATEMENT

Accession For	
NTIS GRA&I	<input checked="checked" type="checkbox"/>
DDC TAB	<input type="checkbox"/>
Unannounced	<input type="checkbox"/>
Justification	
By _____	
Distribution/	
Availability Codes	
Dist..	Avail and/or special
<b>A</b>	

DISTRIBUTION STAMP



DATE ACCESSIONED

79 06 27 315

DATE RECEIVED IN DDC

PHOTOGRAPH THIS SHEET

RETURN TO DDA-2

INFLUENCE OF STRONG SELF ELECTRIC FIELDS ON THE ION RESONANCE INSTABILITY  
IN A NONNEUTRAL PLASMA COLUMN

Ronald C. Davidson\*  
Division of Magnetic Fusion Energy  
Energy Research and Development Administration  
Washington, D. C. 20545

Hwan-sup Uhm  
Department of Physics and Astronomy  
University of Maryland, College Park, Md. 20742

The influence of strong self-electric fields on the ion resonance instability is examined for a cylindrical nonneutral plasma column immersed in a uniform axial magnetic field  $B_0 \hat{e}_z$ . The analysis is carried out within the framework of a macroscopic cold-fluid model, and electrostatic stability properties are investigated for the case of rectangular electron and ion density profiles. The parameter  $\delta = (2\omega_{pe}^2 / \omega_{ce}^2)(1-f)$  is introduced as a convenient measure of the relative strengths of the equilibrium self-electric force and the magnetic force on an electron fluid element. (Here,  $\omega_{pe}$  is the electron plasma frequency,  $\omega_{ce}$  is the electron cyclotron frequency,  $f = n_i^0 / n_e^0$  is the fractional charge neutralization, and  $\delta=1$  corresponds to the maximum allowed charge density for radial confinement of the equilibrium configuration.) An important conclusion of this study is that the equilibrium self-electric field can have a large influence on stability behavior. In particular, stability properties for  $\delta \lesssim 1$  differ substantially from those obtained when  $\delta \ll 1$ . Moreover, for a nonneutral plasma column with significant charge neutralization, it is found that the fundamental mode ( $\ell=1$ ) is not the most unstable mode. Rather, higher harmonic perturbations have larger growth rates. However, in the limiting case where  $f \ll 1$  and  $\delta \ll 1$ , the  $\ell=1$  mode can have the largest growth rate, which is consistent with the result previously obtained by Levy et al.

\*On leave of absence from the University of Maryland, College Park, Md.

# 1. INTRODUCTION

There have been several recent experimental and theoretical studies of the fundamental equilibrium and stability properties of nonneutral plasmas<sup>1</sup> in both mirror<sup>2-5</sup> and uniform<sup>6-10</sup> magnetic field configurations. Perhaps one of the most basic instabilities that characterizes a nonneutral plasma with both electron and ion components is the ion resonance instability.<sup>11-13</sup> In cylindrical geometry (Fig. 1), the ion resonance instability can be described as a two-rotating-stream instability<sup>11</sup> in which the relative rotation between electrons and ions is produced by the equilibrium self-electric field  $E_r^0(r)\hat{e}_r$ . Previous analyses<sup>11,12</sup> of this instability have been restricted to low beam densities and small values of fractional charge neutralization, i.e.,

$$\frac{2\hat{\omega}_{pe}^2}{\omega_{ce}^2} (1-f) \ll 1, \quad f \ll 1.$$

Here,  $\hat{\omega}_{pe}$  is the electron plasma frequency,  $\omega_{ce}$  is the electron cyclotron frequency, and  $f = n_i^0/n_e^0$  is the fractional charge neutralization provided by the positive ion background. In this paper, we investigate the influence of strong self-electric fields on the ion resonance instability in a nonneutral plasma column with rectangular electron and ion density profiles (Fig. 2). The analysis is carried out within the framework of a macroscopic model, treating the electrons and ions as cold ( $T_j \rightarrow 0$ ) fluids immersed in a uniform axial magnetic field  $B_0\hat{e}_z$ . Moreover, the stability studies assume electrostatic perturbations with infinitely long axial wavelength ( $\partial/\partial z = 0$ ).

It is useful to introduce the dimensionless parameter

$$\delta \equiv \frac{2\omega_{pe}^2}{\omega_{ce}^2} (1-f) ,$$

which is a measure of the characteristic relative strength of the equilibrium self-electric force and the magnetic force on an electron fluid element. In the present equilibrium and stability analysis, the parameter  $\delta$  and the fractional charge neutralization  $f$  are allowed to span the range of values

$$0 < \delta \leq 1 ,$$

and

$$0 \leq f \leq 1 ,$$

where  $\delta=1$  corresponds to the maximum allowed charge density for radial confinement of the equilibrium configuration. One of the most important conclusions of this study is that the equilibrium self-electric field can have a large influence on stability behavior. In particular, stability properties for  $\delta \lesssim 1$  differ substantially from those obtained when  $\delta \ll 1$  (see, for example, Fig. 5). Moreover, for a nonneutral plasma column with significant charge neutralization, it is found that the fundamental mode ( $\ell=1$ ) is not the most unstable mode. Rather, higher harmonic perturbations have larger growth rates (see, for example, Figs. 8 and 9). However, in the special limiting case where  $f \ll 1$  and  $\delta \ll 1$ , the  $\ell=1$  mode can have the largest growth rate, which is consistent with the result previously obtained by Levy et al.<sup>12</sup> [Fig. 8].

The outline of this paper is the following. In Section 2, we give a brief description of the theoretical model (Section 2.A) and summarize the equilibrium properties for general density profiles  $n_j^0(r)$ ,  $j=e,i$  (Section 2.B). The corresponding eigenvalue equation

79 00 27 315

that describes the electrostatic stability properties of the nonneutral plasma column is derived in Section 3.A [Eq. (13)]. In Sections 3.B and 3.C, the eigenvalue equation is solved for the case where the electron and ion density profiles are rectangular [Eqs. (20)-(22)]. This leads to a fourth-order algebraic dispersion relation that determines the complex eigenfrequency  $\omega$  [Eq. (26)]. A detailed numerical analysis of the dispersion relation is presented in Section 4, where stability properties are investigated for a broad range of plasma parameters  $\hat{\omega}_{pe}^2/\omega_{ce}^2$ ,  $f$ , etc.

Finally, we emphasize that the present analysis is based on a macroscopic cold-fluid model in which the ion (and electron) motion is assumed to be laminar. Although this is a reasonable approximation when  $r_{Li} \ll R_p$  (where  $r_{Li}$  is the characteristic thermal ion Larmor radius, and  $R_p$  is the radius of the plasma column), we expect significant modifications to the stability behavior when  $r_{Li} \sim R_p$ . The influence of finite ion Larmor radius effects on the ion resonance instability is currently under investigation<sup>14</sup> within the framework of a hybrid Vlasov-fluid model, which treats the electrons as a macroscopic, cold fluid and the ions in a fully kinetic (Vlasov) manner.

## 2. THEORETICAL MODEL AND EQUILIBRIUM PROPERTIES

### 2.A Theoretical Model

As illustrated in Fig. 1, the equilibrium configuration consists of a cylindrically symmetric nonneutral plasma column that is infinite in axial extent and aligned parallel to a uniform applied magnetic field  $B_0 \hat{e}_z$ . The mean motion of the plasma components is in the azimuthal direction, and the applied magnetic field provides radial confinement of the plasma column. As shown in Fig. 1, the characteristic radius of the plasma column is denoted by  $R_p$ , and we introduce a cylindrical polar coordinate system  $(r, \theta, z)$  with the  $z$  axis coinciding with the axis of symmetry;  $r$  is the radial distance from the  $z$  axis, and  $\theta$  is the polar angle in a plane perpendicular to the  $z$  axis. The deviation from equilibrium charge neutrality  $[n_e^0(r) \neq n_i^0(r)]$  produces an equilibrium radial electric field  $E_r^0(r) \hat{e}_r$  that influences the azimuthal motion of the plasma components.

The following are the main assumptions pertaining to the equilibrium and stability analysis:

(a) Equilibrium properties are independent of  $z$  ( $\partial/\partial z = 0$ ) and azimuthally symmetric ( $\partial/\partial \theta = 0$ ) about the  $z$  axis. For example, the mean equilibrium velocity of component  $j$  ( $j=e, i$ ) can be expressed as  $v_j^0(\mathbf{r}) = v_{j\theta}^0(r) \hat{e}_\theta$ , where  $\hat{e}_\theta$  is a unit vector in the  $\theta$  direction, and  $\partial v_{j\theta}^0 / \partial \theta = 0 = \partial v_{j\theta}^0 / \partial z$ .

(b) For present purposes, the electrons and ions are treated as cold ( $T_j \rightarrow 0$ ) fluids immersed in the uniform axial magnetic field  $B_0 \hat{e}_z$ . Within the context of the electrostatic approximation ( $\nabla \times \mathbf{E} = 0$  and  $\nabla \times \mathbf{B} = 0$ ), the equation of motion and continuity equation for each plasma component ( $j=e, i$ ) can be expressed as

$$\left(\frac{\partial}{\partial t} + \mathbf{V}_j \cdot \nabla\right) \mathbf{V}_j = \frac{e_j}{m_j} \left( \mathbf{E} + \frac{\mathbf{V}_j \times \mathbf{B}_0 \hat{\mathbf{e}}_z}{c} \right), \quad (1)$$

$$\frac{\partial}{\partial t} n_j + \nabla \cdot (n_j \mathbf{V}_j) = 0, \quad (2)$$

where  $\mathbf{E}(\mathbf{x}, t) = -\nabla\phi(\mathbf{x}, t)$  is the electric field,  $n_j(\mathbf{x}, t)$  is the density,  $\mathbf{V}_j(\mathbf{x}, t)$  is the mean velocity, and  $e_j$  and  $m_j$  are the charge and mass, respectively, of a particle of species  $j$ . In Eq. (1), the spatial variation in  $B_0$  is neglected (low-beta approximation), and the electrostatic potential  $\phi(\mathbf{x}, t)$  is determined self-consistently from Poisson's equation

$$\nabla^2 \phi = 4\pi e(n_e - n_i), \quad (3)$$

where  $-e$  is the electron charge.

(c) In the stability analysis, flute perturbations with  $\partial/\partial z = 0$  are considered. All quantities are expressed as an axisymmetric equilibrium value plus a perturbation, i.e.,  $\psi(\mathbf{x}, t) = \psi_0(r) + \delta\psi(\mathbf{x}, t)$ . Assuming perturbations with azimuthal harmonic number  $\ell$ , the quantity  $\delta\psi(\mathbf{x}, t)$  is then expressed as

$$\delta\psi(\mathbf{x}, t) = \delta\hat{\psi}_\ell(r) \exp[i(\ell\theta - \omega t)], \quad (4)$$

where  $\omega$  is the complex eigenfrequency.

## 2.B General Equilibrium Properties

An equilibrium analysis of Eqs. (1)-(3) for general steady-state ( $\partial/\partial t = 0$ ) profiles,  $n_j^0(r)$ ,  $\mathbf{V}_{j0}^0(r)$  and  $\phi^0(r)$ , proceeds in the following manner. First, it is straightforward to show from Eq. (2) that the functional form of the density profile  $n_j^0(r)$  can be specified arbitrarily. Moreover, from Eq. (1), equilibrium force balance in the

radial direction can be expressed as  $-m_j V_{j\theta}^{02}(r)/r = e_j E_r^0(r) + e_j V_{j\theta}^0(r) B_0/c$ , or equivalently

$$\omega_j^2 + \epsilon_j \omega_{cj} \omega_j - \epsilon_j \omega_E \omega_{cj} = 0, \quad (5)$$

where  $\epsilon_j = \text{sgn} e_j$ ,  $\omega_{cj} = |e_j| B_0 / m_j c$  is the cyclotron frequency,  $\omega_j(r) = V_{j\theta}^0(r)/r$  is the angular velocity of a fluid element, and  $\omega_E(r)$  is the angular  $E \times B_0$  frequency defined by

$$\omega_E = - \frac{c}{r B_0} E_r^0 = \frac{c}{r B_0} \frac{\partial}{\partial r} \phi^0. \quad (6)$$

Finally, the equilibrium electrostatic potential  $\phi^0(r)$  is determined self-consistently from the steady-state Poisson equation

$$\frac{1}{r} \frac{\partial}{\partial r} r \frac{\partial}{\partial r} \phi^0 = 4\pi e (n_e^0 - n_i^0), \quad (7)$$

where  $n_e^0(r)$  and  $n_i^0(r)$  are the equilibrium electron and ion density profiles. We note from Eq. (5) that there are two allowed equilibrium values of  $\omega_j$ . Solving Eq. (5) for  $\omega_j$  gives

$$\omega_j = \omega_j^\pm \equiv - \frac{\epsilon_j \omega_{cj}}{2} \left[ 1 \pm \left( 1 + 4\epsilon_j \frac{\omega_E}{\omega_{cj}} \right)^{1/2} \right], \quad (8)$$

where the upper sign ( $\omega_j = \omega_j^+$ ) corresponds to a "fast" rotational equilibrium, and the lower sign ( $\omega_j = \omega_j^-$ ) corresponds to a "slow" rotational equilibrium. Evidently, in the limit of equilibrium charge neutrality with  $\omega_E = 0$ , it follows from Eq. (5) that  $\omega_j^+ = -\epsilon_j \omega_{cj}$  and  $\omega_j^- = 0$ .

### 3. ELECTROSTATIC STABILITY PROPERTIES

#### 3.A General Eigenvalue Equation

To investigate electrostatic stability behavior, we make use of Eq. (4) and linearize Eqs. (1)-(3) about the axisymmetric equilibrium state characterized by  $n_j^0(r)$ ,  $V_j^0(x) = \omega_j(r) r \hat{e}_\theta$ , and  $E_\kappa^0(x) = -(\partial\phi^0/\partial r) \hat{e}_r$ .

This readily gives

$$-i(\omega - \ell\omega_j) \delta \hat{V}_{jr} - (\epsilon_j \omega_{cj} + 2\omega_j) \delta \hat{V}_{j\theta} = -\frac{e_j}{m_j} \frac{\partial}{\partial r} \delta \hat{\phi}, \quad (9)$$

$$-i(\omega - \ell\omega_j) \delta \hat{V}_{j\theta} + [\epsilon_j \omega_{cj} + \frac{1}{r} \frac{\partial}{\partial r} (r^2 \omega_j)] \delta \hat{V}_{jr} = -\frac{e_j}{m_j} \frac{1}{r} \delta \hat{\phi}, \quad (10)$$

$$-i(\omega - \ell\omega_j) \delta \hat{n}_j + \frac{1}{r} \frac{\partial}{\partial r} (r n_j^0 \delta \hat{V}_{jr}) + \frac{1}{r} \frac{\partial}{\partial r} (r n_j^0 \delta \hat{V}_{j\theta}) = 0, \quad (11)$$

$$\frac{1}{r} \frac{\partial}{\partial r} r \frac{\partial}{\partial r} \delta \hat{\phi} - \frac{\ell^2}{r^2} \delta \hat{\phi} = -4\pi \sum_j e_j \delta \hat{n}_j, \quad (12)$$

where the index  $\ell$  has been suppressed on the perturbation amplitudes  $\delta \hat{V}_{jr}(r)$ ,  $\delta \hat{\phi}(r)$ , etc. It is evident from Eqs. (9)-(11) that the perturbations in density and mean fluid velocities can be expressed directly in terms of  $\delta \hat{\phi}(r)$ . After some straightforward algebra, Eq. (12)

becomes

$$\begin{aligned} & \frac{1}{r} \frac{\partial}{\partial r} \left[ r \left( 1 - \sum_j \frac{\omega_{pj}^2}{v_j^2} \right) \frac{\partial}{\partial r} \delta \hat{\phi} \right] \\ & - \frac{\ell^2}{r^2} \left( 1 - \sum_j \frac{\omega_{pj}^2}{v_j^2} \right) \delta \hat{\phi} \\ & = -\frac{\ell \delta \hat{\phi}}{r} \sum_j \frac{1}{\omega - \ell\omega_j} \frac{\partial}{\partial r} \left( \frac{\omega_{pj}^2}{v_j^2} (\epsilon_j \omega_{cj} + 2\omega_j) \right), \end{aligned} \quad (13)$$

where  $\omega_{pj}^2(r) = 4\pi n_j^0(r) e_j^2 / m_j$ , and  $v_j^2(r)$  is defined by

$$v_j^2(r) = (\omega - \ell\omega_j)^2 - (\epsilon_j \omega_{cj} + 2\omega_j) \left( \epsilon_j \omega_{cj} + \frac{1}{r} \frac{\partial}{\partial r} (r^2 \omega_j) \right). \quad (14)$$

The eigenvalue equation (13) can be used to calculate the eigenfunction

$\delta\hat{\phi}(r)$  and complex eigenfrequency  $\omega$  for a broad class of equilibrium profiles  $n_j^0(r)$  and  $\omega_j(r)$  consistent with Eqs. (5)-(8).

### 3.B Eigenvalue Equation for Sharp-Boundary Equilibrium

For present purposes, we specialize to the case where the electron and ion density profiles are rectangular [Fig. 2], i.e.,

$$n_e^0(r) = \begin{cases} n_0 = \text{const.}, & 0 < r < R_p, \\ 0 & , R_p < r < R_c, \end{cases} \quad (15)$$

and

$$n_i^0(r) = \begin{cases} fn_0 = \text{const.}, & 0 < r < R_p, \\ 0 & , R_p < r < R_c, \end{cases} \quad (16)$$

where  $f = \text{const.} = \text{fractional charge neutralization}$ , and  $r = R_c$  is the radial location of a grounded conducting wall. From Eqs. (7), (15) and (16), we find  $\phi^0(r) = \pi en_0(1-f)r^2$  inside the plasma column ( $0 < r < R_p$ ). Making use of Eq. (6), the equilibrium  $E_v^0 \times B_0$  frequency can be expressed as

$$\omega_E = \frac{2\pi en_0 c}{B_0} (1-f) = \text{const.} \quad (17)$$

Substituting Eq. (17) into Eq. (8) gives

$$\omega_e = \omega_e^{\pm} = \frac{\omega_{ce}}{2} \left[ 1 \pm \left( 1 - \frac{2\hat{\omega}_{pe}^2}{\omega_{ce}^2} (1-f) \right)^{1/2} \right], \quad (18)$$

and

$$\omega_i = \omega_i^{\pm} = -\frac{\omega_{ci}}{2} \left[ 1 \pm \left( 1 + \frac{m_i}{m_e} \frac{2\hat{\omega}_{pe}^2}{\omega_{ce}^2} (1-f) \right)^{1/2} \right], \quad (19)$$

where  $\hat{\omega}_{pe}^2 = 4\pi n_0 e^2 / m_e$ . It is evident from Eqs. (18) and (19) that the angular velocity profiles  $\omega_e$  and  $\omega_i$  are uniform (independent of  $r$ ) for the electron and ion density profiles illustrated in Fig. 2.

For the rectangular density profiles prescribed by Eqs. (15) and (16), the eigenvalue equation (13) can be expressed as

$$\begin{aligned} \frac{1}{r} \frac{\partial}{\partial r} \left[ r \left( 1 - \sum_j \frac{\omega_{pj}^2}{v_j^2} \right) \frac{\partial}{\partial r} \delta \hat{\phi} \right] - \frac{\ell^2}{r^2} \left( 1 - \sum_j \frac{\omega_{pj}^2}{v_j^2} \right) \delta \hat{\phi} \\ = \frac{\ell \delta \hat{\phi}}{r} \sum_j \frac{\omega_{pj}^2}{v_j^2} \frac{\epsilon_j \omega_{cj} + 2\omega_j}{\omega - \ell \omega_j} \delta(r - R_p) \end{aligned} \quad (20)$$

where

$$v_j^2(r) = (\omega - \ell \omega_j)^2 - (\epsilon_j \omega_{cj} + 2\omega_j)^2 = \text{const.} \quad (21)$$

and

$$\omega_{pj}^2(r) = \begin{cases} \hat{\omega}_{pj}^2 = \text{const.}, & 0 < r < R_p, \\ 0 & R_p < r < R_c. \end{cases} \quad (22)$$

In Eqs. (20) and (22),  $\hat{\omega}_{pe}^2 = 4\pi n_0 e^2 / m_e$  and  $\hat{\omega}_{pi}^2 = 4\pi f n_0 e^2 / m_i$ , and use has been made of  $\partial \omega_{pj}^2 / \partial r = -\hat{\omega}_{pj}^2 \delta(r - R_p)$ .

### 3.C Dispersion Relation for Sharp-Boundary Equilibrium

Except at the point  $r = R_p$ , it is clear from Eqs. (20)-(22) that  $\delta \hat{\phi}(r)$  satisfies the vacuum Poisson equation  $r^{-1}(\partial/\partial r)[r \partial \delta \hat{\phi} / \partial r] - (\ell^2/r^2) \delta \hat{\phi} = 0$ . Therefore, the solution to Eq. (20) can be expressed as

$$\delta \hat{\phi}_i(r) = A(r/R_p)^\ell, \quad 0 \leq r < R_p, \quad (23)$$

inside the plasma column, and

$$\delta \hat{\phi}_o(r) = A \left( \frac{r}{R_p} \right)^\ell \frac{(1 - R_c^{2\ell}/r^{2\ell})}{(1 - R_c^{2\ell}/R_p^{2\ell})}, \quad R_p < r < R_c, \quad (24)$$

in the vacuum region between the surface of the plasma column and the conducting wall. Note that the perturbed potential is continuous at the surface of the plasma column with  $\delta \hat{\phi}_i(r = R_p) = \delta \hat{\phi}_o(r = R_p) = A$ . Moreover, the perturbed potential vanishes at the conducting wall,

i.e.,  $\delta\hat{\phi}_0(r=R_c)=0$ .

The dispersion relation that determines the complex eigenfrequency  $\omega$  is obtained by multiplying Eq. (20) by  $r$  and integrating from  $R_p(1-\epsilon)$  to  $R_p(1+\epsilon)$ , with  $\epsilon \rightarrow 0_+$ . This gives

$$\begin{aligned} R_p \left( \frac{\partial}{\partial r} \delta\hat{\phi}_0 \right)_{r=R_p} - R_p \left( 1 - \sum_j \frac{\hat{\omega}_{pj}^2}{v_j^2} \right) \left( \frac{\partial}{\partial r} \delta\hat{\phi}_1 \right)_{r=R_p} \\ = \ell \delta\hat{\phi}(r=R_p) \sum_j \frac{\hat{\omega}_{pj}^2}{v_j^2} \frac{\epsilon_j \omega_{cj} + 2\omega_j}{\omega - \ell\omega_j}. \end{aligned} \quad (25)$$

Substituting Eqs. (23) and (24) into Eq. (25) and rearranging terms, we obtain

$$0 = \frac{1}{1-(R_p/R_c)^{2\ell}} - \sum_j \frac{\hat{\omega}_{pj}^2}{2(\omega - \ell\omega_j) [(\omega - \ell\omega_j) + (\epsilon_j \omega_{cj} + 2\omega_j)]}. \quad (26)$$

Throughout the remainder of this article, we assume that the electron and ion equilibria are rotating in the "slow" rotational mode with

$$\omega_e = \omega_e^-, \quad \text{and} \quad \omega_i = \omega_i^-. \quad (27)$$

In this case, Eq. (26) can be expressed as

$$\begin{aligned} 0 = \frac{1}{1-(R_p/R_c)^{2\ell}} - \frac{\hat{\omega}_{pe}^2}{2(\omega - \ell\omega_e^-) [(\omega - \ell\omega_e^-) - (\omega_e^+ - \omega_e^-)]} \\ - \frac{\hat{\omega}_{pi}^2}{2(\omega - \ell\omega_i^-) [(\omega - \ell\omega_i^-) - (\omega_i^+ - \omega_i^-)]}, \end{aligned} \quad (28)$$

where  $\omega_e^\pm$  and  $\omega_i^\pm$  are defined in Eqs. (18) and (19). The linear dispersion relation (28) can be used to investigate electrostatic stability properties for a broad range of plasma parameters  $f$ ,  $\hat{\omega}_{pe}^2/\omega_{ce}^2$ , etc.

As a point of reference, we note that the ion resonance instability has previously been studied in the low-density, low-frequency regime

characterized by<sup>11,12</sup>

$$\frac{\hat{\omega}_{pe}^2}{\omega_{ce}^2} (1-f) \ll 1, \quad (29)$$

$$|\omega - \ell\omega_e^-| \ll |\omega_e^+ - \omega_e^-|.$$

Within the context of the inequalities in Eq. (29), the linear dispersion relation (28) can be approximated by

$$0 = \frac{1}{1 - (R_p/R_c)^2} + \frac{\hat{\omega}_{pe}^2}{2\omega_{ce}(\omega - \ell\omega_e^-)} - \frac{\hat{\omega}_{pi}^2}{2(\omega - \ell\omega_i^-)[(\omega - \ell\omega_i^-) - (\omega_i^+ - \omega_i^-)]}, \quad (30)$$

where use has been made of  $\omega_e^- \approx \omega_E$  and  $\omega_e^+ - \omega_e^- \approx \omega_{ce}$  [Eqs. (17), (18)

and (29)]. Equation (30) is identical to the dispersion relation obtained by Levy et al.<sup>11</sup> within the framework of a fluid model

in which the electron motion is approximated by  $\mathbf{v}_e = c(\mathbf{E} \times \hat{\mathbf{e}}_z)/B_0$ .

Throughout the remainder of this article, Eq. (30) is referred to as the "reference dispersion relation" (RDR). In order to assess the influence of strong self electric fields on stability behavior [ $2(\hat{\omega}_{pe}^2/\omega_{ce}^2)(1-f) \leq 1$ ], it will be useful, from time to time, to

compare the stability information obtained from the unexpanded

dispersion relation (28) with that obtained from Eq. (30). In this

regard, we emphasize that the inequalities in Eq. (29) pose a particularly

severe limitation on the range of validity of Eq. (30). The present

paper is intended to alleviate this situation by a thorough investigation of the unexpanded dispersion relation (28).

### 3.D Dimensionless Parameters

It is evident from Eqs. (17)-(19) and the linear dispersion relation (28) that the four dimensionless parameters

$$\frac{\hat{\omega}_{pe}^2}{\omega_{ce}^2}, \quad f, \quad \frac{m_e}{m_i}, \quad \frac{R_p}{R_c}, \quad (31)$$

can be used to characterize the plasma equilibrium. Moreover, an important dimensionless parameter that measures the strength of the equilibrium electric force on an electron fluid element is [Eq. (8)]

$$\delta \equiv 4 \frac{\omega_E}{\omega_{ce}} = \frac{2\hat{\omega}_{pe}^2}{\omega_{ce}^2} (1-f), \quad (32)$$

which can be constructed from the dimensionless parameters in Eq. (31).

Because

$$\frac{2\hat{\omega}_{pe}^2}{\omega_{ce}^2} (1-f) \leq 1 \quad (33)$$

is necessarily required for existence of the electron equilibrium [Eq. (18)], we note from Eqs. (32) and (33) that  $\delta$  can span the range  $0 \leq \delta \leq 1$ .

For future convenient reference, in Fig. 3 are shown plots of  $\omega_E/\omega_{ce}$  [Eq. (17)],  $\omega_e^\pm/\omega_{ce}$  [Eq. (18)] and  $\omega_i^\pm/\omega_{ci}$  [Eq. (19)] versus the dimensionless parameter  $\delta = (2\hat{\omega}_{pe}^2/\omega_{ce}^2)(1-f)$  for  $m_e/m_i = 1/1836$ .

In the limit of maximum charge density for existence of the equilibrium ( $\delta=1$ ), we note from Fig. 3 that  $\omega_i^\pm/\omega_{ci} \approx \mp(m_i/4m_e)^{1/2}$  and  $\omega_e^\pm/\omega_{ce} = 0.5$ .

Finally, in Fig. 4, we illustrate the region of the parameter

space  $(f, \hat{\omega}_{pe}^2/\omega_{ce}^2)$  corresponding to existence of the equilibrium

[Eq. (33)]. Note that the equilibrium electron density can exceed the Brillouin flow limit ( $\hat{\omega}_{pe}^2/\omega_{ce}^2 = 0.5$ ) provided there is sufficient

charge neutralization that  $f \geq 1 - 0.5(\omega_{ce}^2 / \hat{\omega}_{pe}^2)$ .

#### 4. STABILITY ANALYSIS

The growth rate  $\gamma = \text{Im}\omega$  and real oscillation frequency  $\omega_r = \text{Re}\omega$  have been obtained numerically from Eq. (28) for a broad range of plasma parameters  $f$ ,  $\hat{\omega}_{pe}^2 / \omega_{ce}^2$  and  $R_p / R_c$ . In this section, we summarize the essential features of these stability studies. The analysis is restricted to nonneutral proton-electron plasmas ( $m_i / m_e = 1836$ ), and the growth rate and real frequency are measured in units of the lower hybrid frequency

$$\omega_{LH} = (\omega_{ce} \omega_{ci})^{1/2}.$$

In order to illustrate the need for an improved dispersion relation at large beam densities, Fig. 5 shows a plot of the normalized growth rate  $\gamma / \omega_{LH}$  and oscillation frequency  $\omega_r / \omega_{LH}$  versus  $\hat{\omega}_{pe}^2 / \omega_{ce}^2$  obtained from Eq. (28) (the unexpanded dispersion relation) and Eq. (30) (the reference dispersion relation), for  $\ell=2$ ,  $R_p / R_c = 0.5$  and  $f=0.45$ . Note that  $\omega_r / \omega_{LH}$  is plotted only for the range of  $\hat{\omega}_{pe}^2 / \omega_{ce}^2$  corresponding to instability ( $\gamma > 0$ ). Moreover, the abscissa in Fig. 5 extends to  $\hat{\omega}_{pe}^2 / \omega_{ce}^2 = 0.91$ , since physically allowed equilibria exist for  $\hat{\omega}_{pe}^2 / \omega_{ce}^2 < 0.5 / (1 - 0.45) = 0.91$  [Eq. (33) and Fig. 4]. Several points are noteworthy in Fig. 5. First, the unexpanded dispersion relation (28) predicts instability for  $0 < \hat{\omega}_{pe}^2 / \omega_{ce}^2 < 0.34$ , whereas the reference dispersion relation (30) predicts instability for the entire range of allowed equilibrium density,  $0 < \hat{\omega}_{pe}^2 / \omega_{ce}^2 < 0.91$ . Second, the maximum growth rate can be a substantial fraction of  $\omega_{LH}$ . In particular, for the parameters assumed in Fig. 5, the maximum

growth rate obtained from Eq. (28) is  $\gamma_{\text{MAX}} = 0.36 \omega_{\text{LH}}$ , which occurs for  $\hat{\omega}_{\text{pe}}^2 / \omega_{\text{ce}}^2 = 0.24$ . Finally, it is evident from Fig. 5 that the reference dispersion relation (30) breaks down at rather modest values of beam density ( $\hat{\omega}_{\text{pe}}^2 / \omega_{\text{ce}}^2 > 0.1$ ), thereby underlining the need for the improved dispersion relation in Eq. (28). Throughout the remainder of this section, the stability analysis is based entirely on Eq. (28).

Stability boundaries in the parameter space  $(f, \hat{\omega}_{\text{pe}}^2 / \omega_{\text{ce}}^2)$  are illustrated in Figs. 6 and 7. In Fig. 6, the solid curves correspond to the stability boundaries ( $\gamma=0$ ) obtained from Eq. (28) for  $\ell=1$ , and several values of  $R_p/R_c$ . For a given value of  $R_p/R_c$ , the region of  $(f, \hat{\omega}_{\text{pe}}^2 / \omega_{\text{ce}}^2)$  parameter space above the curve corresponds to instability ( $\gamma>0$ ), whereas the region of parameter space below the curve corresponds to stability ( $\gamma=0$ ). For low beam densities (small values of  $\hat{\omega}_{\text{pe}}^2 / \omega_{\text{ce}}^2$ ), it is evident from Fig. 6 that the system is stable for  $\ell=1$ , provided  $R_p/R_c$  is sufficiently small. On the other hand, for high beam densities, wall stabilization occurs provided  $R_p/R_c$  is sufficiently large, i.e., provided the conducting wall is located sufficiently close to the plasma surface. In Fig. 7, the solid curves correspond to the stability boundaries obtained from Eq. (28) for  $R_p/R_c=0.5$  and several values of azimuthal mode number  $\ell$ . For a given density of physical interest ( $\hat{\omega}_{\text{pe}}^2 / \omega_{\text{ce}}^2 > 0.01$ , say), we note that the number of unstable modes increases rapidly as the fractional charge neutralization  $f$  is increased to sufficiently large values.

The dependence of stability properties on fractional charge neutralization is further illustrated in Figs. 8 and 9 where the normalized growth rate  $\gamma/\omega_{\text{LH}}$  and oscillation frequency  $\omega_r/\omega_{\text{LH}}$  are

plotted versus  $f$  for  $\hat{\omega}_{pe}^2/\omega_{ce}^2=0.01$  (Fig. 8) and  $\hat{\omega}_{pe}^2/\omega_{ce}^2=0.5$  (Fig. 9), and several values of mode number  $\ell$ . Also,  $R_p/R_c=0.5$  is assumed in Figs. 8 and 9. In Figs. 8(b) and 9(b),  $\omega_r/\omega_{LH}$  is plotted only for the ranges of  $f$  corresponding to instability ( $\gamma>0$ ). Note the rapid increase in the number of unstable modes when  $f$  is increased to sufficiently large values. Several important features are evident from Figs. 8 and 9. First, for the low-density case illustrated in Fig. 8 ( $\hat{\omega}_{pe}^2/\omega_{ce}^2=0.01$ ), we note that only the fundamental mode ( $\ell=1$ ) is unstable when  $f<0.13$ . This is consistent with the results previously obtained by Levy et al. for  $\hat{\omega}_{pe}^2/\omega_{ce}^2, f\ll 1$ . Second, the maximum growth rate for each mode number  $\ell$  is a slowly increasing function of  $f$ . Evidently, as the fractional charge neutralization  $f$  approaches unity, the number of unstable modes tends to infinity within the context of the present cold-fluid model. Moreover, in the limit of equilibrium charge neutrality ( $f=1$ ), the self electric field is equal to zero and the plasma column is stable ( $\gamma=0$  in Figs. 8 and 9). Finally, for low beam densities, we note that the real frequency  $\omega_r$  exhibits a nearly linear dependence on fractional charge neutralization  $f$  (Fig. 8). In contrast, when the equilibrium self-electric field is sufficiently large (Fig. 9),  $\omega_r$  exhibits a strongly nonlinear dependence on  $f$ .

Shown in Figs. 10 and 11 are plots of normalized growth rate  $\gamma/\omega_{LH}$  and oscillation frequency  $\omega_r/\omega_{LH}$  versus  $\hat{\omega}_{pe}^2/\omega_{ce}^2$  for  $f=0.1$  (Fig. 10) and  $f=0.8$  (Fig. 11), and several values of mode number  $\ell$ . Also,  $R_p/R_c=0.5$  is assumed in Figs. 10 and 11. For small values of fractional charge neutralization, it is evident that the fundamental mode ( $\ell=1$ ) is the most unstable mode. For example, for the  $f=0.1$  case

shown in Fig. 10, the maximum growth rate ( $\gamma_{\text{MAX}} \approx 0.093 \omega_{\text{LH}}$ ) occurs for  $\ell=1$  and  $\hat{\omega}_{\text{pe}}^2/\omega_{\text{ce}}^2 \approx 0.12$ . This is in contrast with Fig. 11, where the maximum growth rate for  $f=0.8$  ( $\gamma_{\text{MAX}} \approx 2.4 \omega_{\text{LH}}$ ) occurs for  $\ell=3$  and  $\hat{\omega}_{\text{pe}}^2/\omega_{\text{ce}}^2 = 2.5$  (the maximum allowed density for radial confinement). Furthermore, for the  $f=0.1$  case shown in Fig. 10, we note that the ion resonance instability is completely stabilized above some critical value of beam density ( $\hat{\omega}_{\text{pe}}^2/\omega_{\text{ce}}^2 > 0.17$ ). On the other hand, for larger values of fractional charge neutralization ( $f=0.8$  in Fig. 11), it is evident that instability exists for the entire allowed range of  $\hat{\omega}_{\text{pe}}^2/\omega_{\text{ce}}^2$ . Moreover, several mode numbers  $\ell$  are unstable for a given value of  $\hat{\omega}_{\text{pe}}^2/\omega_{\text{ce}}^2$ , a feature generally characteristic of a nonneutral plasma column with significant charge neutralization (see also Figs. 7-9).

Of considerable interest for experimental application is the stability behavior for specified values of  $f$ ,  $\hat{\omega}_{\text{pe}}^2/\omega_{\text{ce}}^2$  and  $R_p/R_c$ . Typical results are shown in Figs. 12 and 13 where  $\gamma/\omega_{\text{LH}}$  and  $\omega_r/\omega_{\text{LH}}$  are plotted versus mode number  $\ell$  for  $\hat{\omega}_{\text{pe}}^2/\omega_{\text{ce}}^2 = 0.01$  (Fig. 12) and  $\hat{\omega}_{\text{pe}}^2/\omega_{\text{ce}}^2 = 0.5$  (Fig. 13), and several values of fractional charge neutralization  $f$ . Also,  $R_p/R_c = 0.5$  is assumed in Figs. 12 and 13, and graphical results are presented only for the unstable mode numbers with  $\gamma > 0$ . For the low-density case in Fig. 12, we note that maximum growth occurs for  $\ell=2$  when  $f=0.2$ , and for  $\ell=12$  when  $f=0.8$ . Evidently, for low beam densities, there is a broad spectrum of unstable modes when the fractional charge neutralization is sufficiently large. On the other hand, for higher beam densities, fewer unstable modes are excited. For example, in Fig. 13, maximum growth occurs for  $\ell=1$  when  $f=0.2$ , and for  $\ell=5$  when  $f=0.8$ . Comparing Figs. 12 and 13, we also note that the maximum growth rate (measured in units of  $\omega_{\text{LH}}$ ) is larger in the high-density case (Fig. 13) than in the low-density

case (Fig. 12).

We conclude this section by emphasizing that stability properties also exhibit a sensitive dependence on the location of the conducting wall. This is illustrated in Fig. 14 where the normalized growth rate  $\gamma/\omega_{\text{LH}}$  and oscillation frequency  $\omega_r/\omega_{\text{LH}}$  are plotted versus  $R_p/R_c$  for  $\ell=1$ ,  $\hat{\omega}_{\text{pe}}^2/\omega_{\text{ce}}^2=0.5$ , and several values of fractional charge neutralization  $f$ . Evidently, the  $\ell=1$  mode is stabilized whenever the conducting wall is located sufficiently close to the plasma surface. Moreover, as  $f$  is increased, the conducting wall must be situated even closer to the plasma surface to assure stability. A qualitatively similar dependence of stability behavior on  $R_p/R_c$  is obtained for higher  $\ell$  values.

## 5. SUMMARY AND CONCLUSIONS

In this paper, we have examined the influence of strong self-electric fields on the ion resonance instability in a nonneutral plasma column. The analysis was carried out within the framework of a macroscopic cold-fluid model (Section 2), and electrostatic stability properties were investigated in detail for the case of rectangular electron and ion density profiles (Sections 3 and 4). One of the most important conclusions of this study is that the equilibrium self-electric field can have a large influence on stability behavior. In particular, stability properties for  $\delta \lesssim 1$  differ substantially from those obtained when  $\delta \ll 1$  (see, for example, Fig. 5). Moreover, for a nonneutral plasma column with significant charge neutralization, it is found that the fundamental mode ( $\ell=1$ ) is not the most unstable mode (see, for example, Figs. 8 and 9). However, in the special limiting case where  $f \ll 1$  and  $\delta \ll 1$ , the  $\ell=1$  mode can have the largest growth rate, which is consistent with the result obtained previously by Levy et al.<sup>12</sup>

Finally, we emphasize that the present analysis is based on a macroscopic cold-fluid model in which the ion (and electron) motion is assumed to be laminar. Although this is a reasonable approximation when  $r_{Li} \ll R_p$  (where  $r_{Li}$  is the characteristic thermal ion Larmor radius), we expect significant modifications to the stability behavior when  $r_{Li} \sim R_p$ . The influence of finite ion Larmor radius effects on the ion resonance instability is currently under investigation<sup>14</sup> within the framework of a hybrid Vlasov-fluid model, which treats the electrons as a macroscopic, cold fluid and the ions in a fully kinetic (Vlasov) manner.

ACKNOWLEDGMENTS

This research was supported by the National Science Foundation. The research by one of the authors (H.U.) was supported in part by the Office of Naval Research under the auspices of the University of Maryland-Naval Research Laboratory Joint Program in Plasma Physics.

REFERENCES

1. R. C. Davidson, Theory of Nonneutral Plasmas, (W. A. Benjamin, Reading, Mass., 1974).
2. C. M. Armstrong, D. A. Hammer, and A. W. Trivelpiece, Phys. Lett. 55A, 413 (1976).
3. R. C. Davidson, A. Drobott, and C. A. Kapetanakis, Phys. Fluids 16, 2199 (1973).
4. R. C. Davidson and J. D. Lawson, Part. Accel. 4, 1 (1972).
5. D. Keefe, Part. Accel. 1, 1 (1970).
6. A. J. Theiss, R. A. Mahaffey, and A. W. Trivelpiece, Phys. Rev. Lett. 35, 1436 (1975).
7. R. A. Mahaffey, S. A. Goldstein, R. C. Davidson, and A. W. Trivelpiece, Phys. Rev. Lett. 35, 1439 (1975).
8. J. M. Malmberg and J. S. DeGrassie, Phys. Rev. Lett. 35, 577 (1975).
9. R. C. Davidson and N. A. Krall, Phys. Fluids 13, 1543 (1970).
10. R. C. Davidson, H. Uhm, and S. M. Mahajan, Phys. Fluids 19, 1608 (1976).
11. Ref. 1, pp 62.
12. R. H. Levy, J. D. Daugherty, and O. Buneman, Phys. Fluids 12, 2616 (1969).
13. D. G. Koshkarev and P. R. Zenkevich, Particle Accel. 3, 1 (1972).
14. "Influence of Finite Ion Larmor Radius Effects on the Ion Resonance Instability in a Nonneutral Plasma Column", R. C. Davidson and H. Uhm, manuscript in preparation (1977).

# FIGURE CAPTIONS

- Fig. 1 Equilibrium configuration and coordinate system.
- Fig. 2 Rectangular density profiles for electrons and ions [Eqs. (15) and (16)].
- Fig. 3 Plots of (a)  $\omega_E/\omega_{ce}$  [Eq. (17)], (b)  $\omega_e^\pm/\omega_{ce}$  [Eq. (18)] and (c)  $\omega_i^\pm/\omega_{ci}$  [Eq. (19)] versus  $\delta = (2\hat{\omega}_{pe}^2/\omega_{ce}^2)(1-f)$  for  $m_i/m_e = 1836$ .
- Fig. 4 The shaded region of the parameter space  $(f, \hat{\omega}_{pe}^2/\omega_{ce}^2)$  corresponds to physically allowed equilibria satisfying  $f \geq 1 - \omega_{ce}^2/2\hat{\omega}_{pe}^2$ .
- Fig. 5 Plots of (a) growth rate  $\gamma$  and (b) real frequency  $\omega_r$  versus  $\hat{\omega}_{pe}^2/\omega_{ce}^2$  obtained from Eq. (28) and the reference dispersion relation (30) for  $\ell=2$ ,  $R_p/R_c=0.5$ ,  $f=0.45$  and  $m_i/m_e=1836$ .
- Fig. 6 Stability boundaries [Eq. (28)] in the parameter space  $(f, \hat{\omega}_{pe}^2/\omega_{ce}^2)$  for  $\ell=1$ ,  $m_i/m_e=1836$  and  $R_p/R_c=0.25, 0.5, 0.75$ .
- Fig. 7 Stability boundaries [Eq. (28)] in the parameter space  $(f, \hat{\omega}_{pe}^2/\omega_{ce}^2)$  for  $R_p/R_c=0.5$ ,  $m_i/m_e=1836$  and several values of  $\ell$ .
- Fig. 8 Plots of (a) growth rate  $\gamma$  and (b) real frequency  $\omega_r$  versus  $f$  [Eq. (28)] for  $\hat{\omega}_{pe}^2/\omega_{ce}^2=0.01$ ,  $m_i/m_e=1836$ ,  $R_p/R_c=0.5$  and several values of  $\ell$ .
- Fig. 9 Plots of (a) growth rate  $\gamma$  and (b) real frequency  $\omega_r$  versus  $f$  [Eq. (28)] for  $\hat{\omega}_{pe}^2/\omega_{ce}^2=0.5$ ,  $m_i/m_e=1836$ ,  $R_p/R_c=0.5$  and several values of  $\ell$ .

- Fig. 10 Plots of (a) growth rate  $\gamma$  and (b) real frequency  $\omega_r$  versus  $\hat{\omega}_{pe}^2/\omega_{ce}^2$  [Eq. (28)] for  $f=0.1$ ,  $m_i/m_e=1836$ ,  $R_p/R_c=0.5$  and several values of  $\ell$ .
- Fig. 11 Plots of (a) growth rate  $\gamma$  and (b) real frequency  $\omega_r$  versus  $\hat{\omega}_{pe}^2/\omega_{ce}^2$  [Eq. (28)] for  $f=0.8$ ,  $m_i/m_e=1836$ ,  $R_p/R_c=0.5$  and several values of  $\ell$ .
- Fig. 12 Plots of (a) growth rate  $\gamma$  and (b) real frequency  $\omega_r$  versus  $\ell$  [Eq. (28)] for  $\hat{\omega}_{pe}^2/\omega_{ce}^2=0.01$ ,  $m_i/m_e=1836$ ,  $R_p/R_c=0.5$  and several values of  $f$ .
- Fig. 13 Plots of (a) growth rate  $\gamma$  and (b) real frequency  $\omega_r$  versus  $\ell$  [Eq. (28)] for  $\hat{\omega}_{pe}^2/\omega_{ce}^2=0.5$ ,  $m_i/m_e=1836$ ,  $R_p/R_c=0.5$  and several values of  $f$ .
- Fig. 14 Plots of (a) growth rate  $\gamma$  and (b) real frequency  $\omega_r$  versus  $R_p/R_c$  [Eq. (28)] for  $\hat{\omega}_{pe}^2/\omega_{ce}^2=0.5$ ,  $\ell=1$ ,  $m_i/m_e=1836$ , and several values of  $f$ .

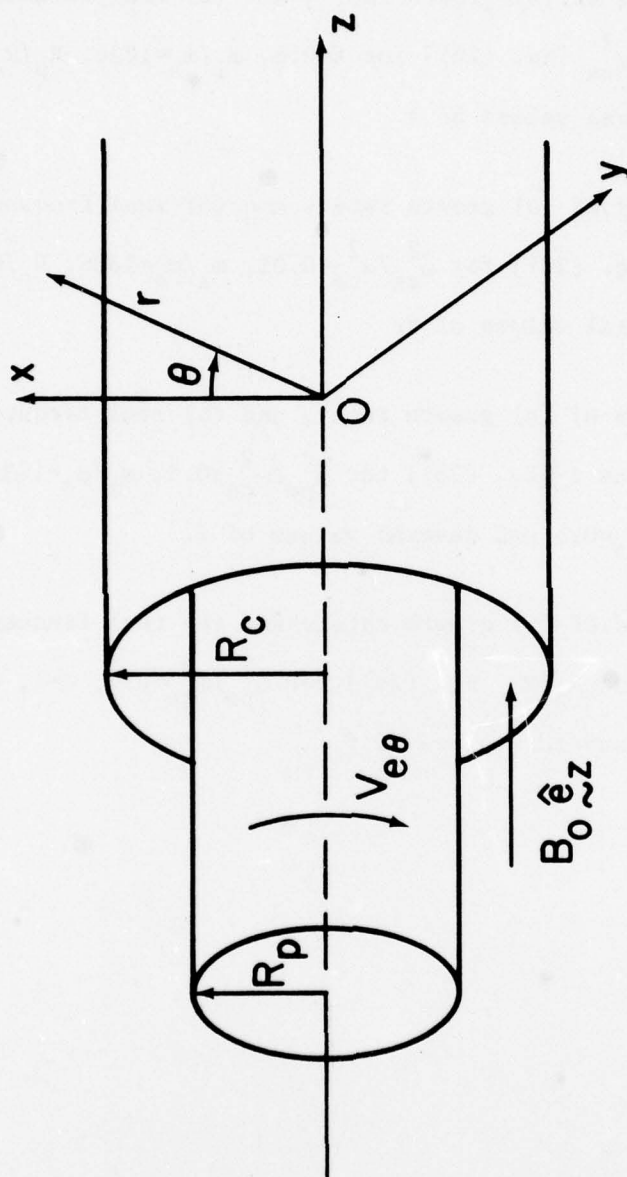


Fig. 1

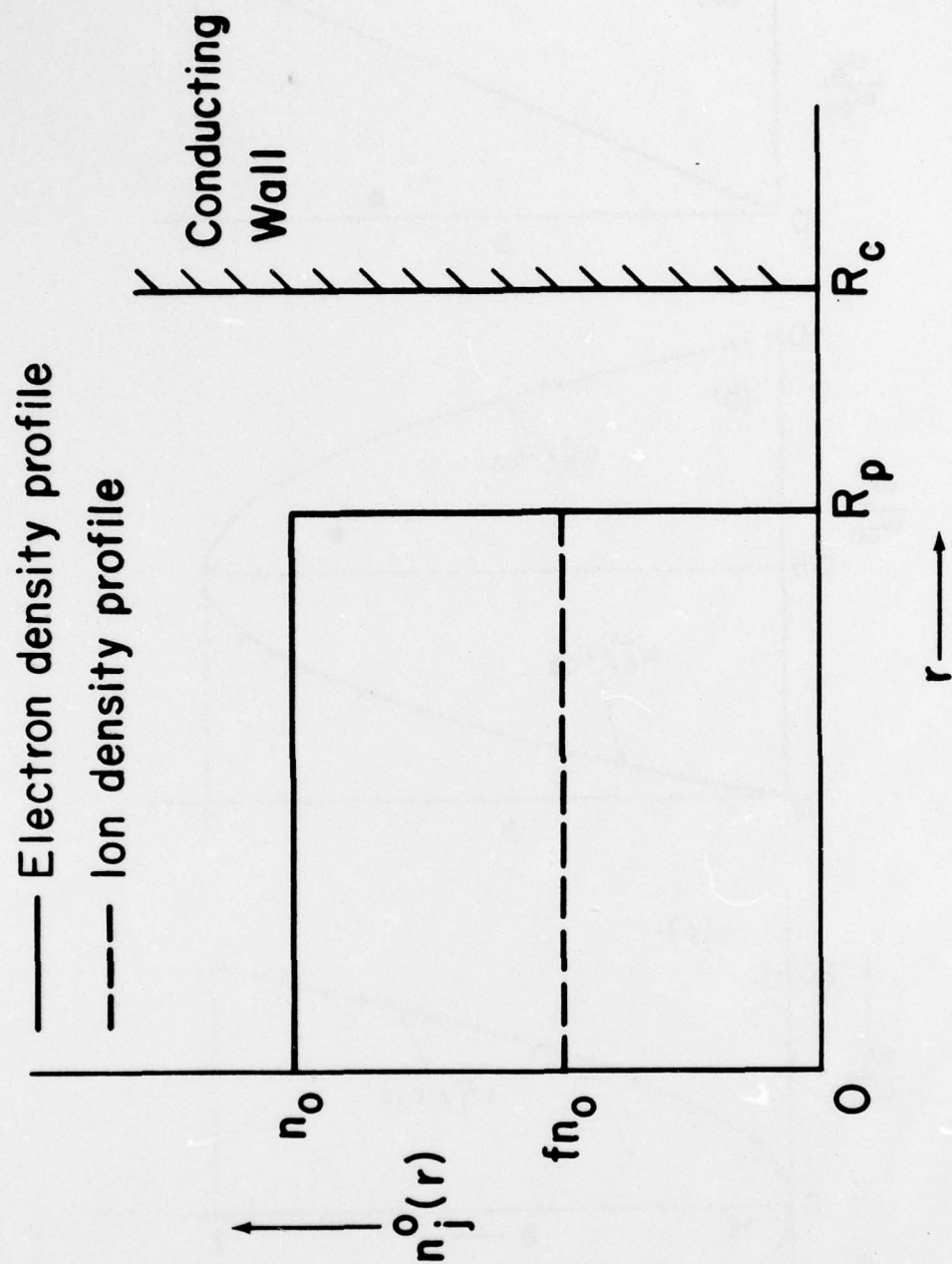


Fig. 2

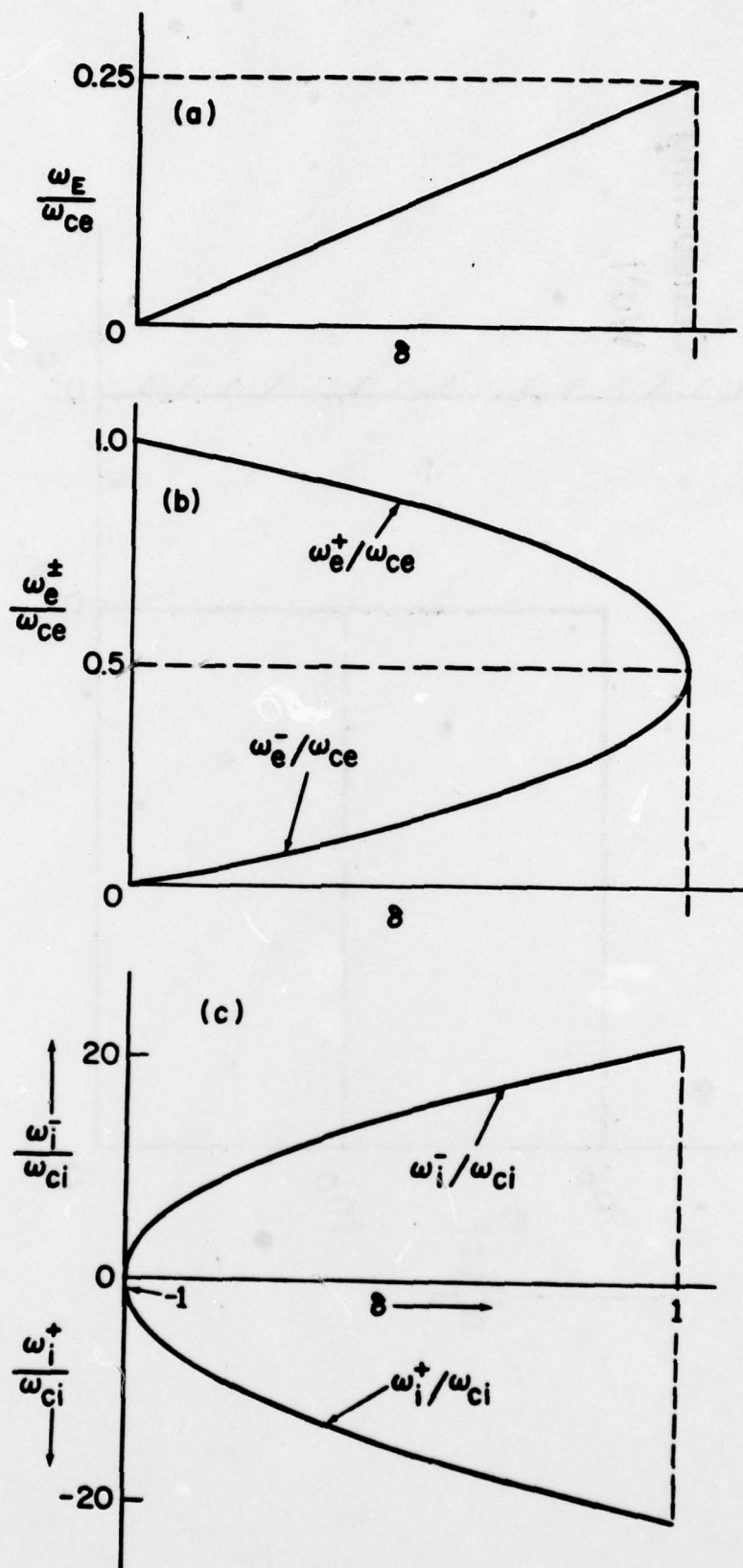


Fig. 3

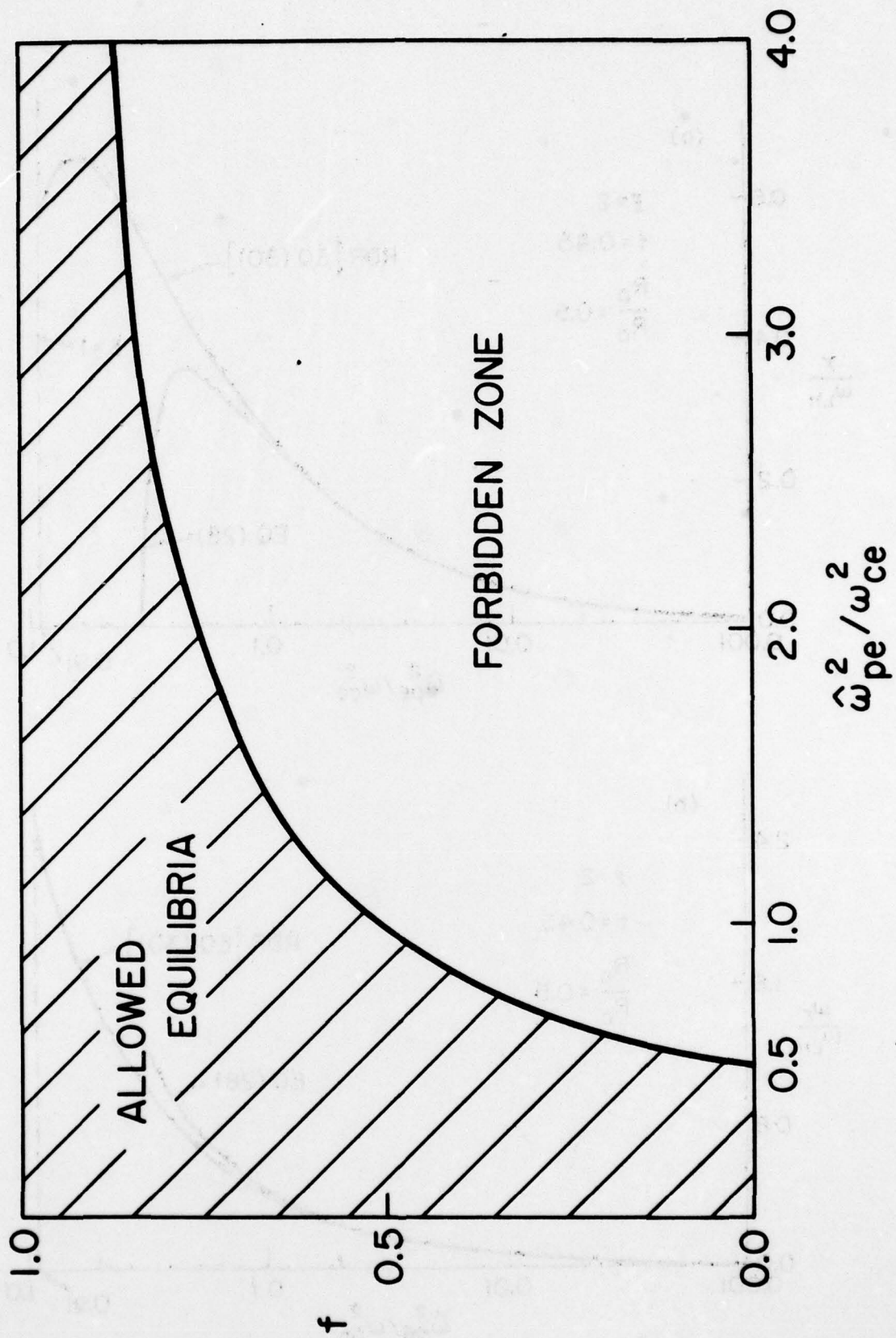


Fig. 4

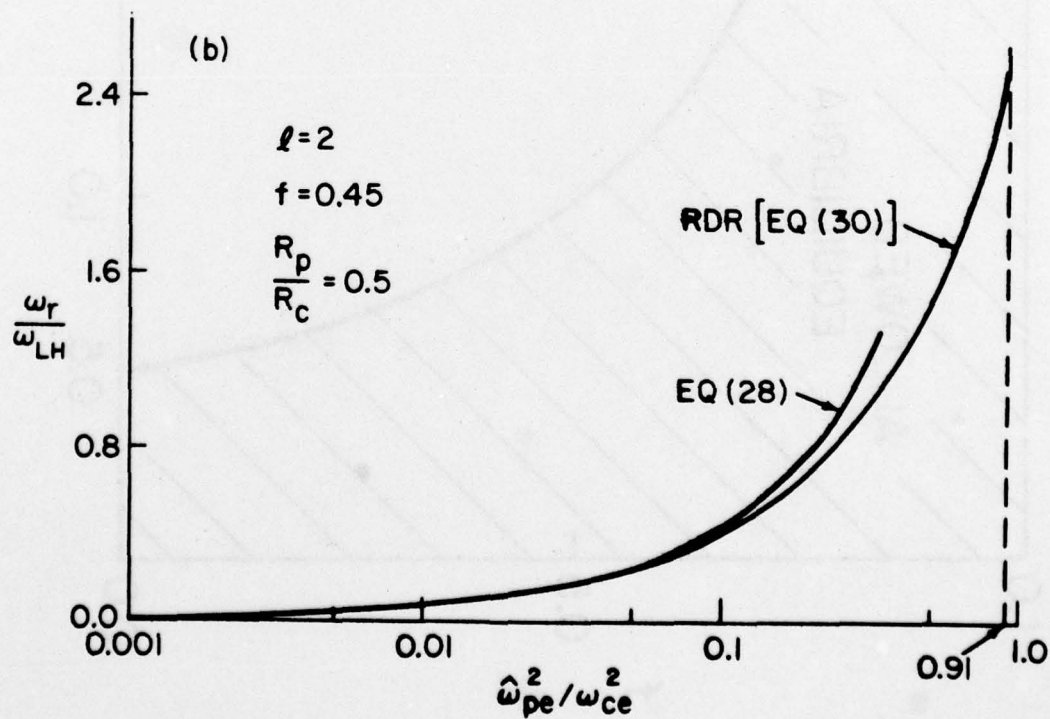
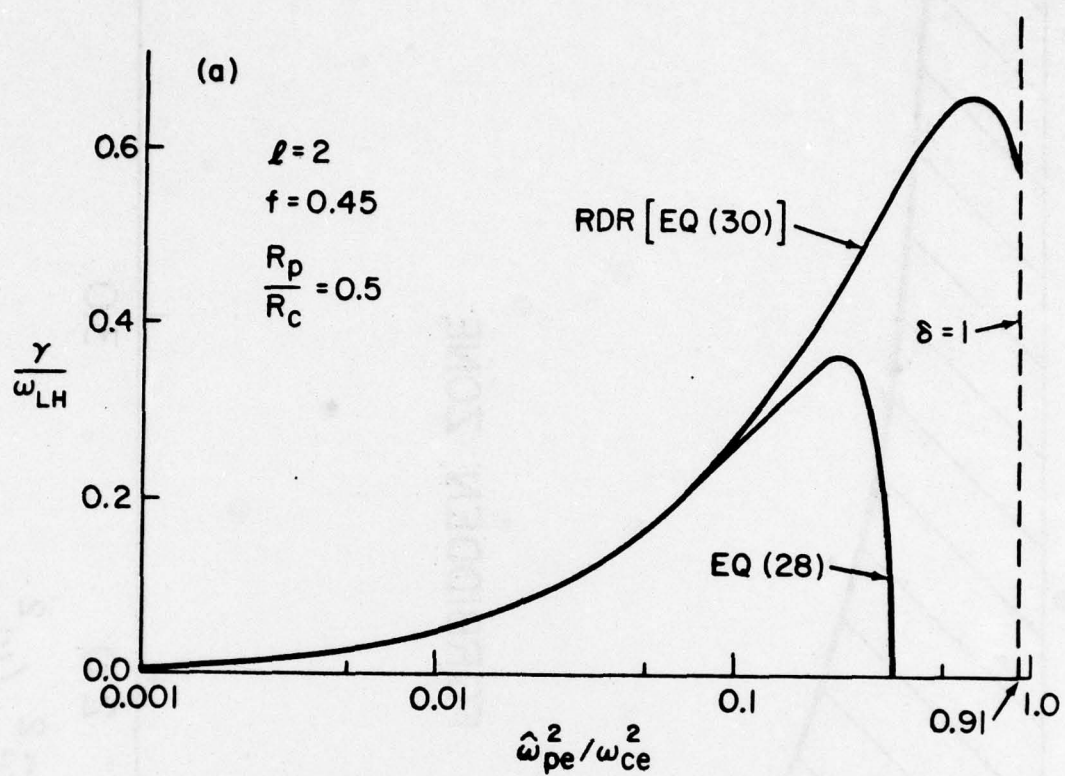


Fig. 5

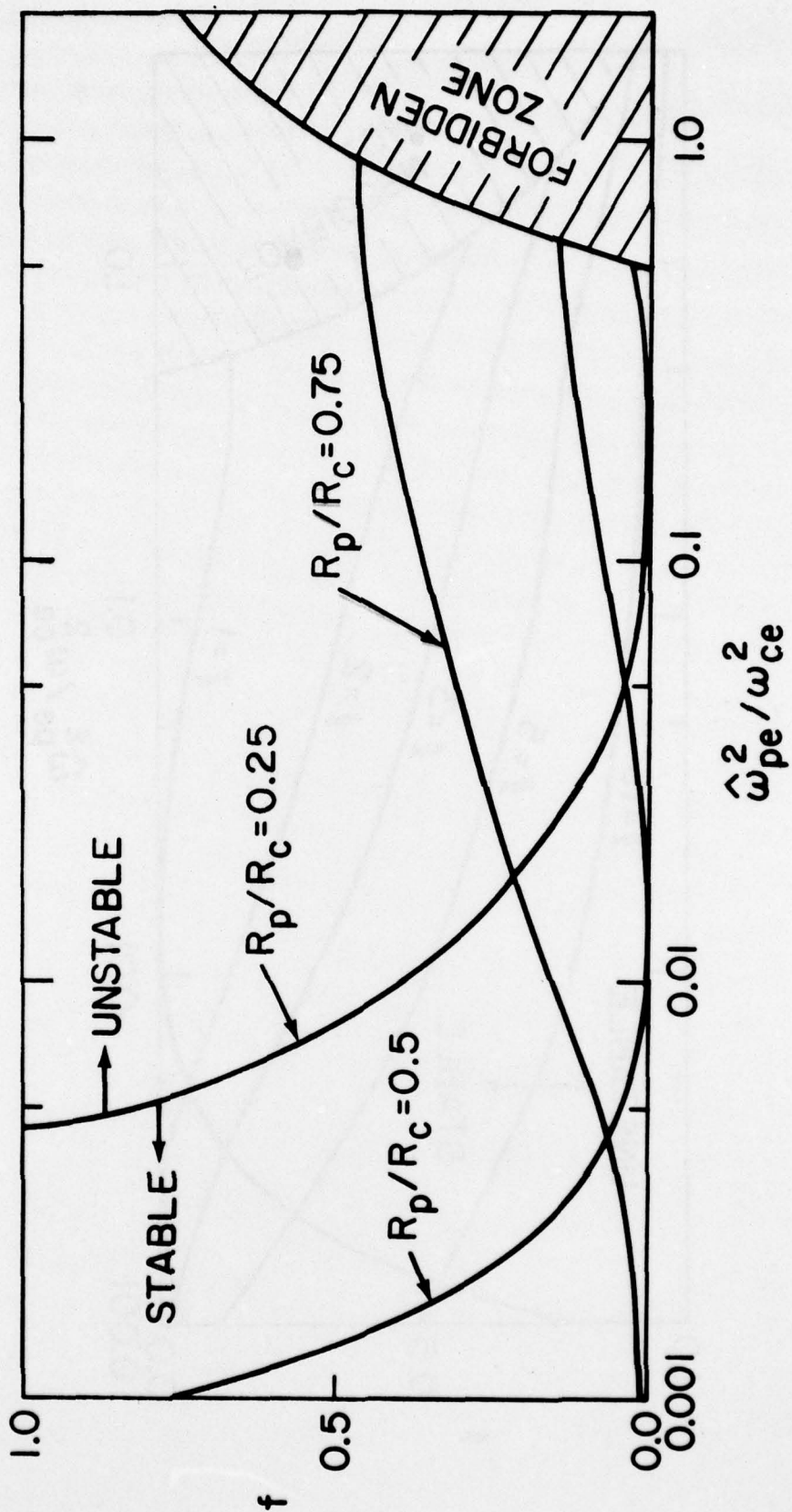


Fig. 6

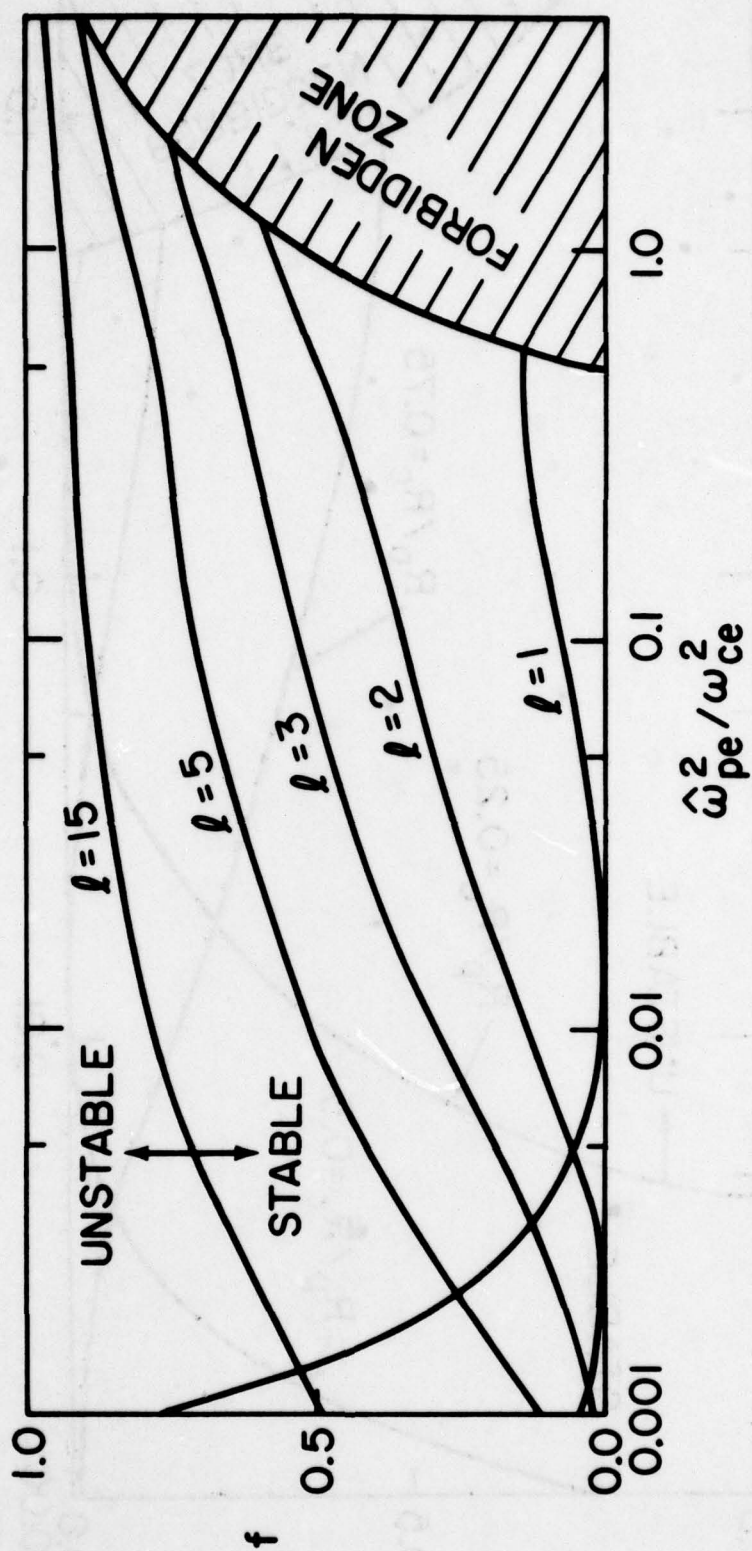


Fig. 7

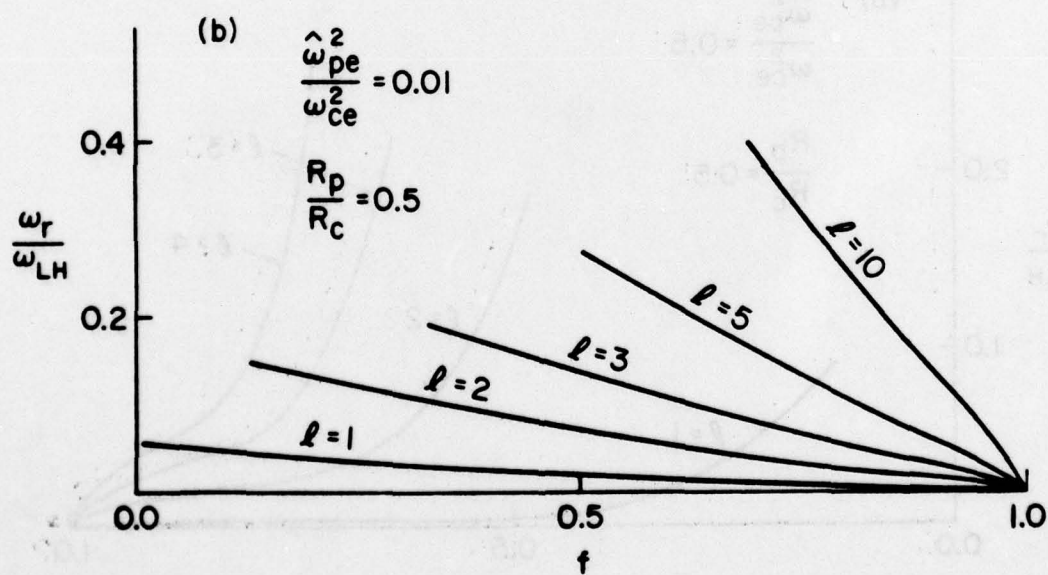
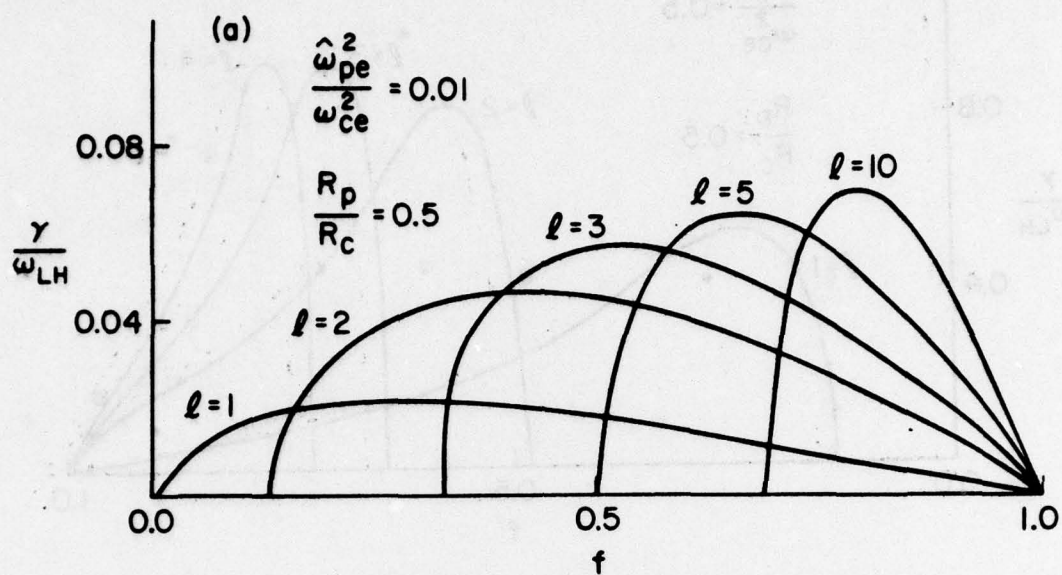


Fig. 8

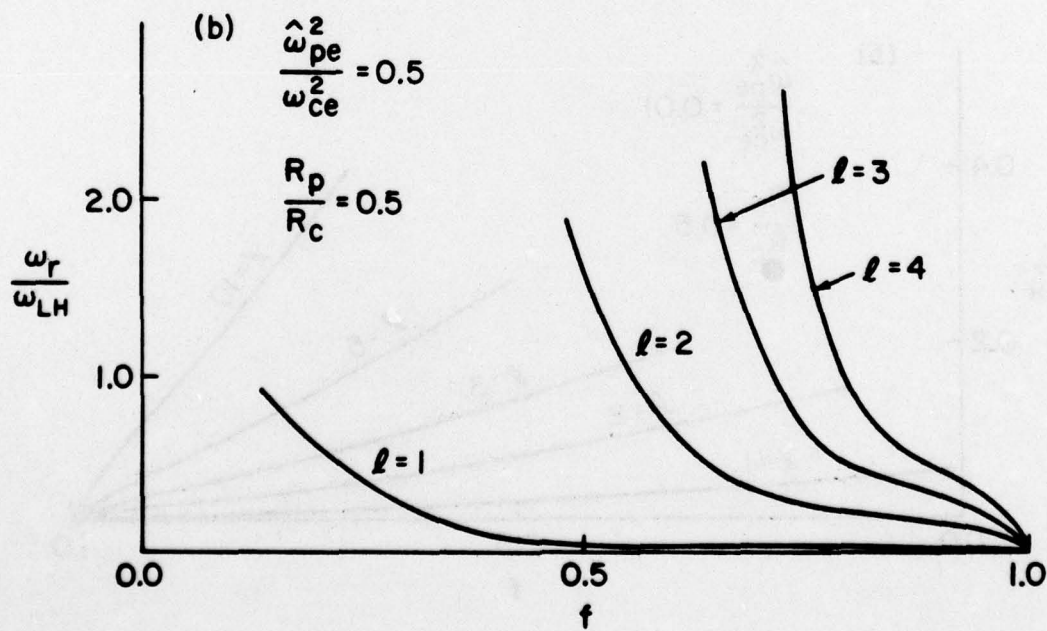
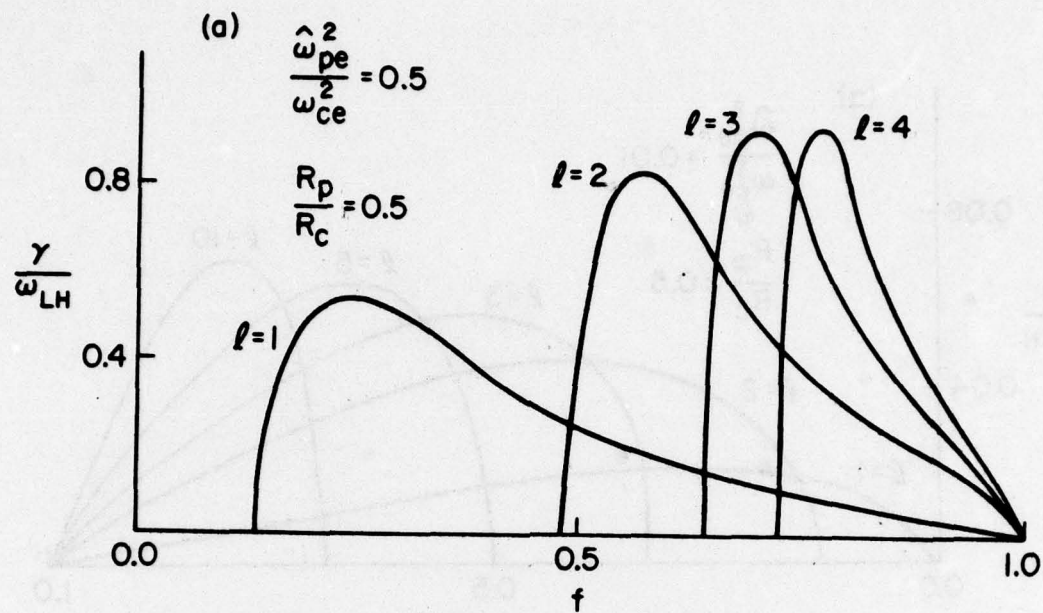


Fig. 9

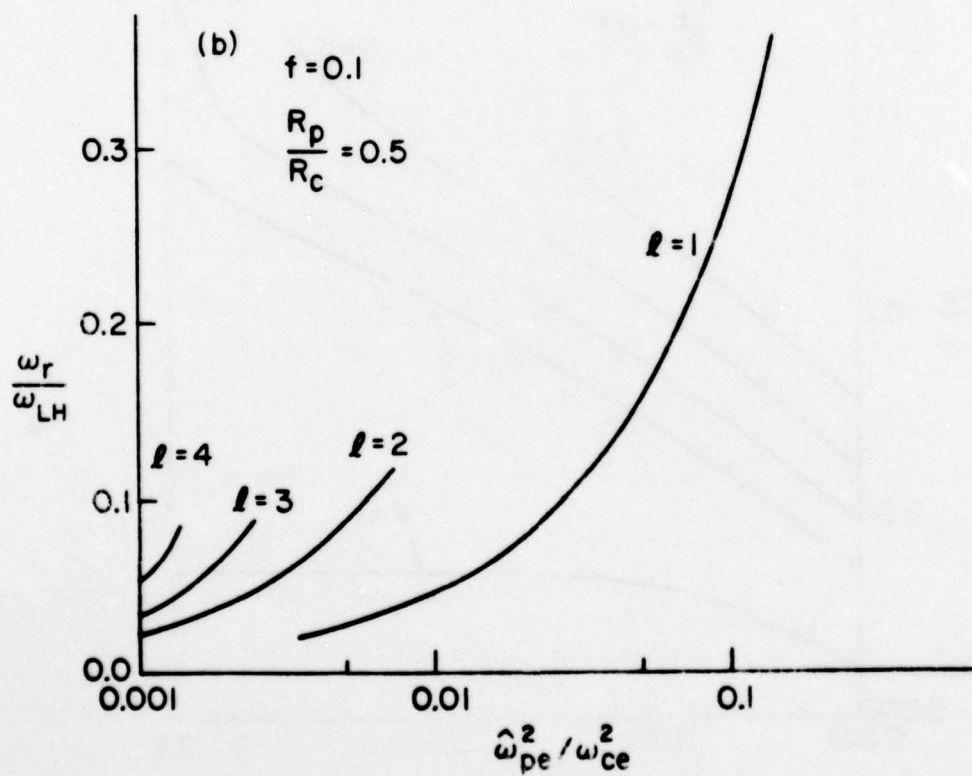
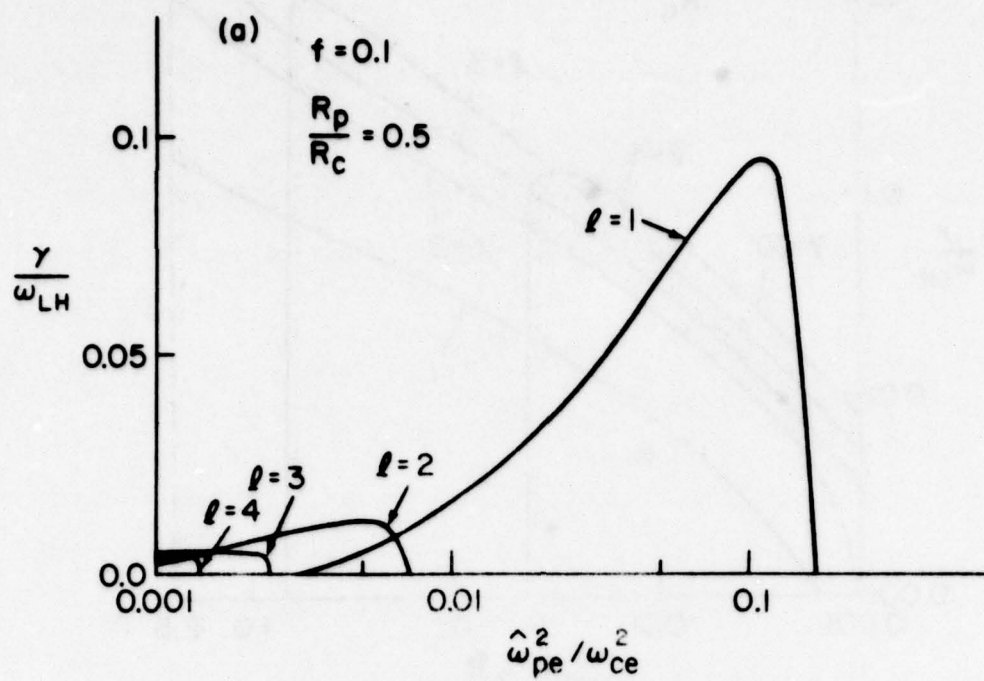
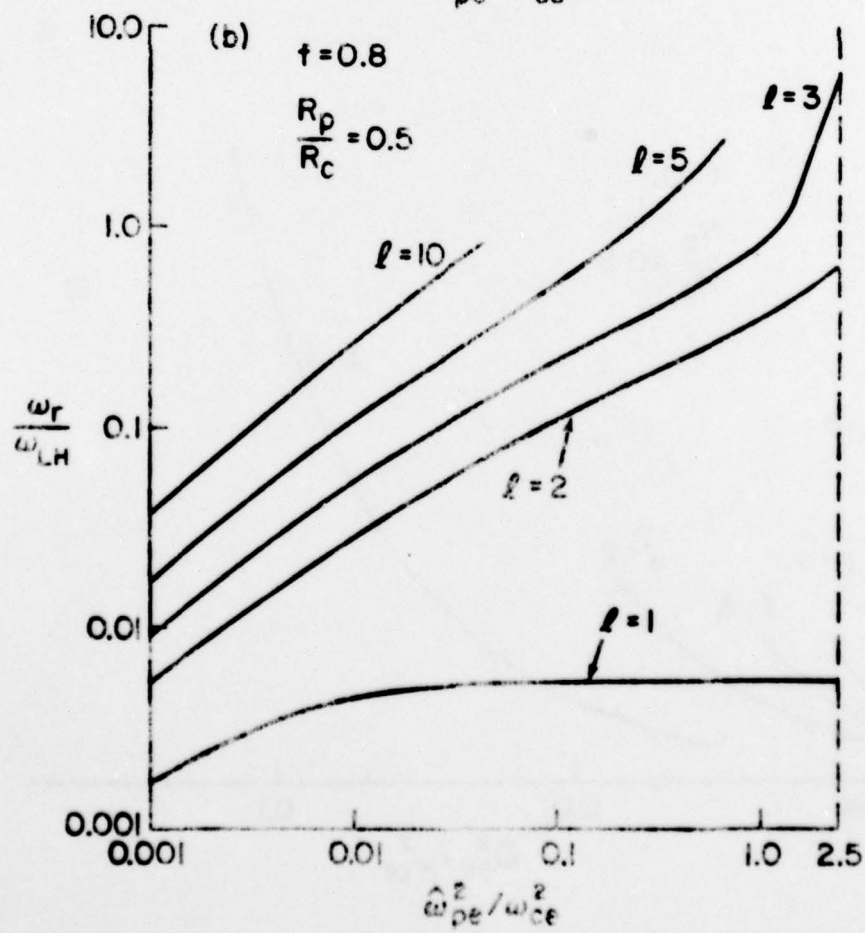
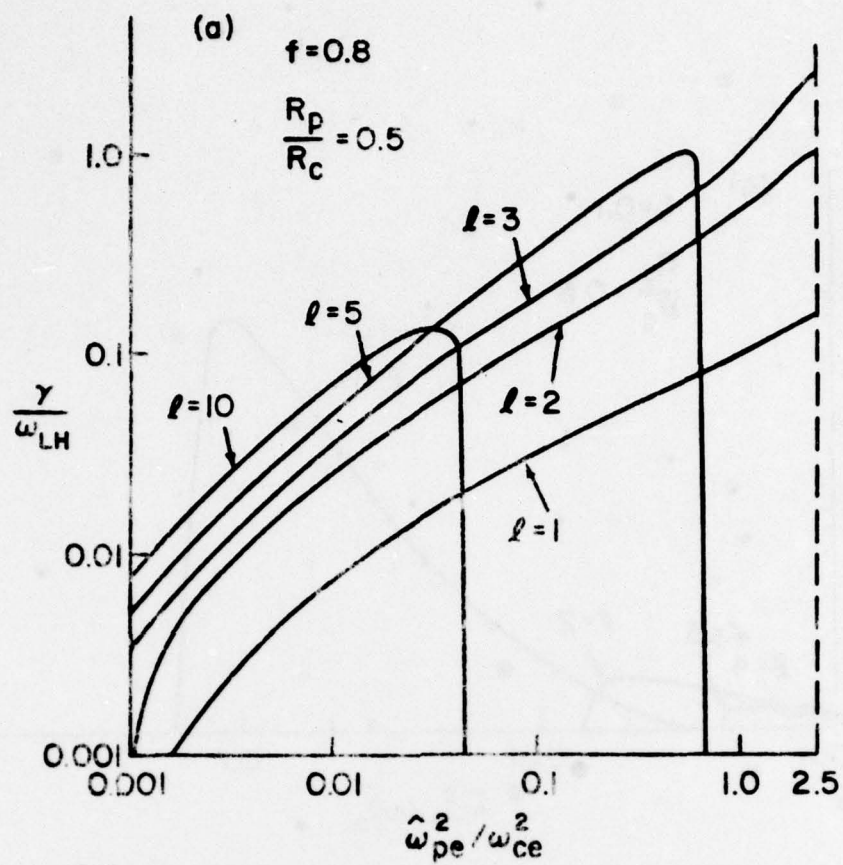


Fig. 10



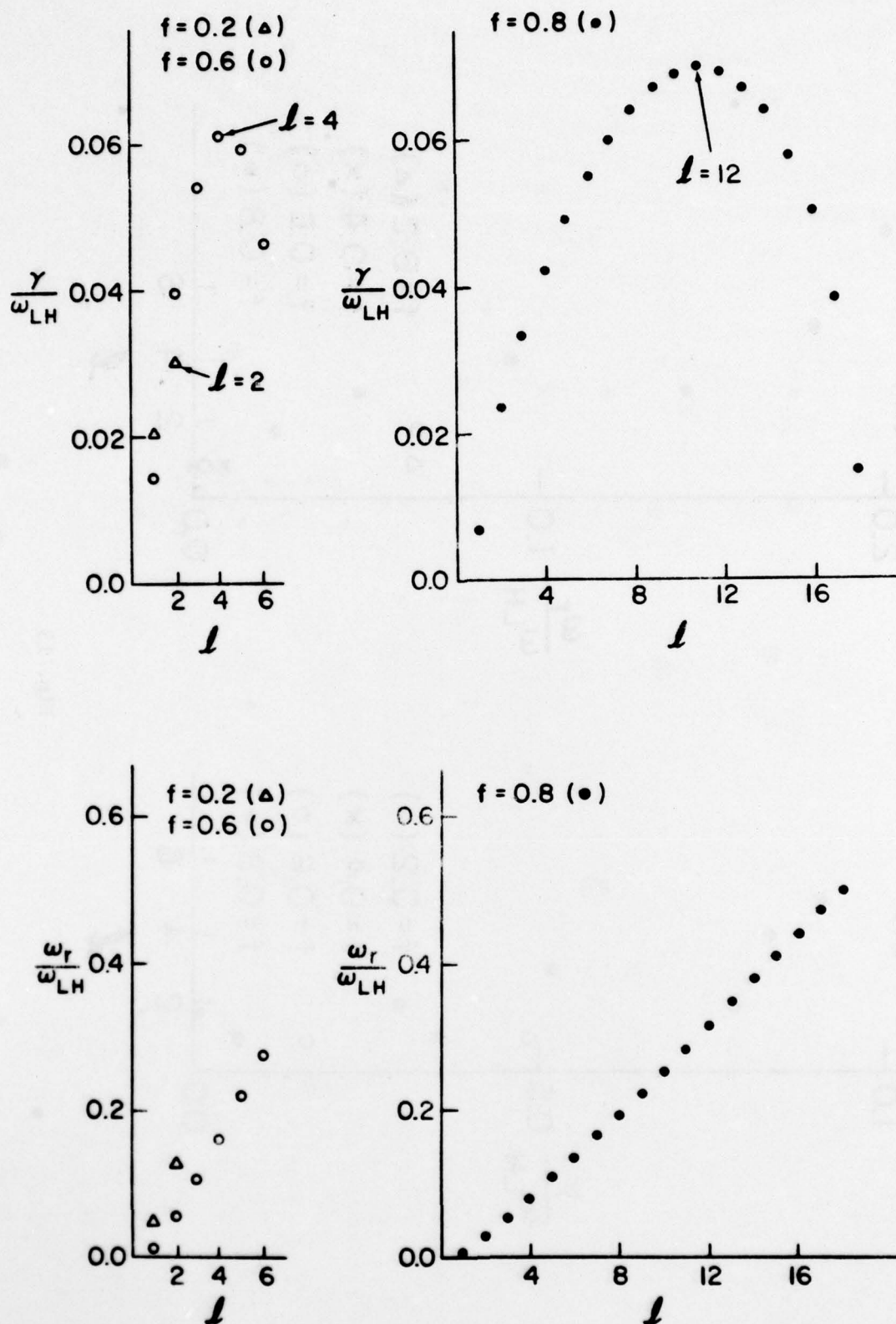


Fig. 12

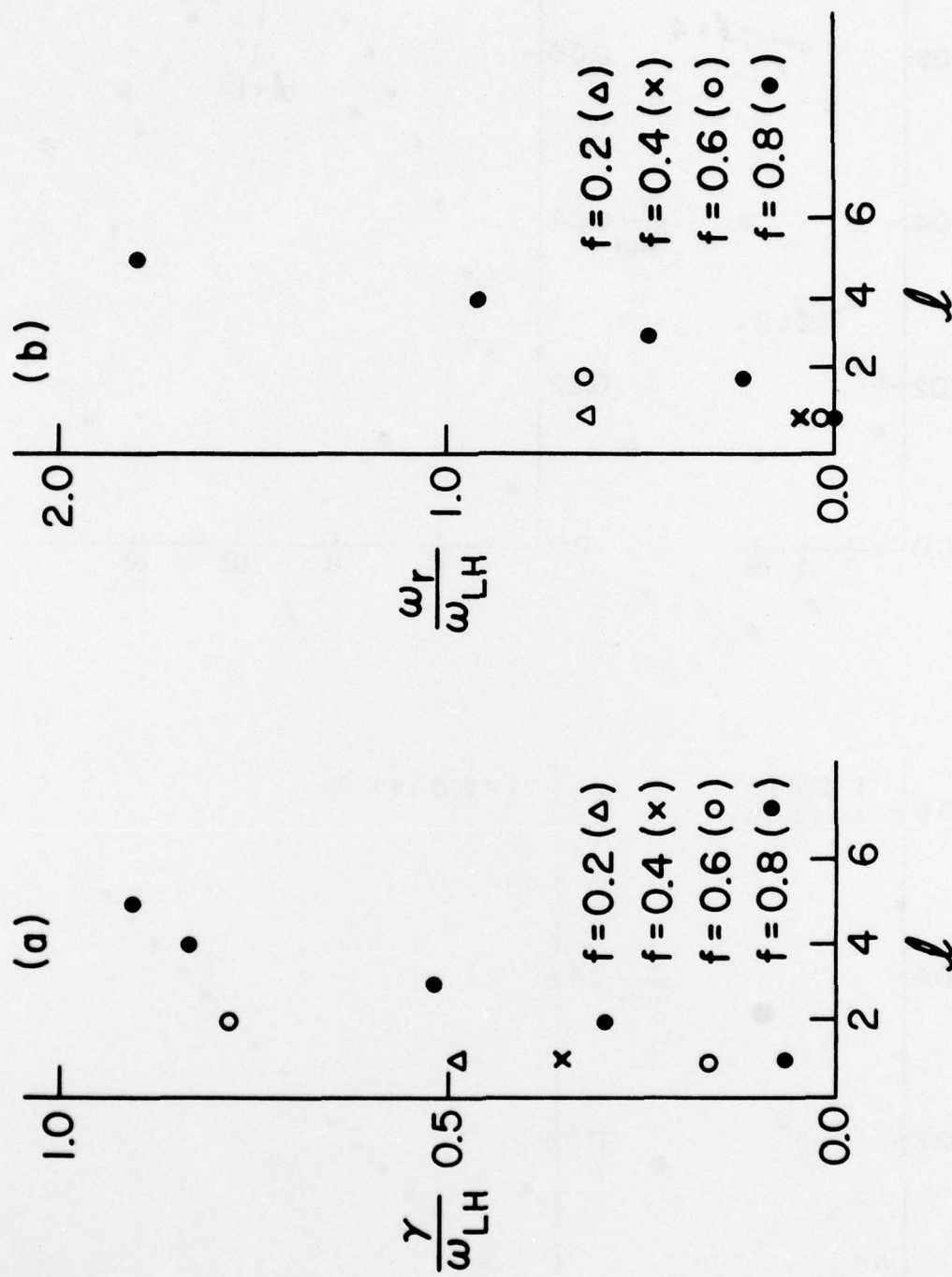


Fig. 13

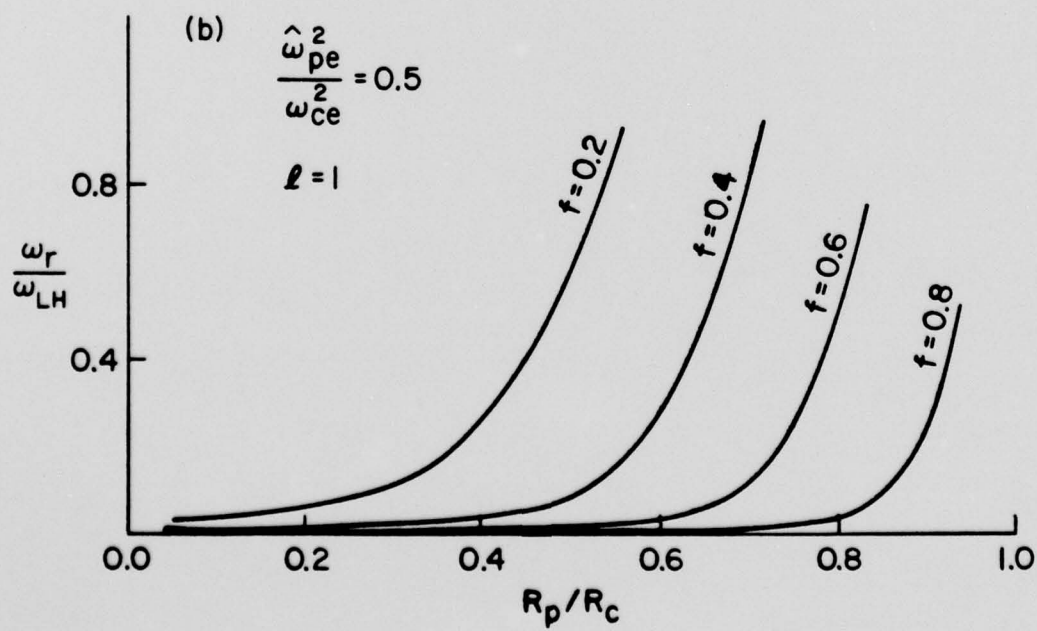
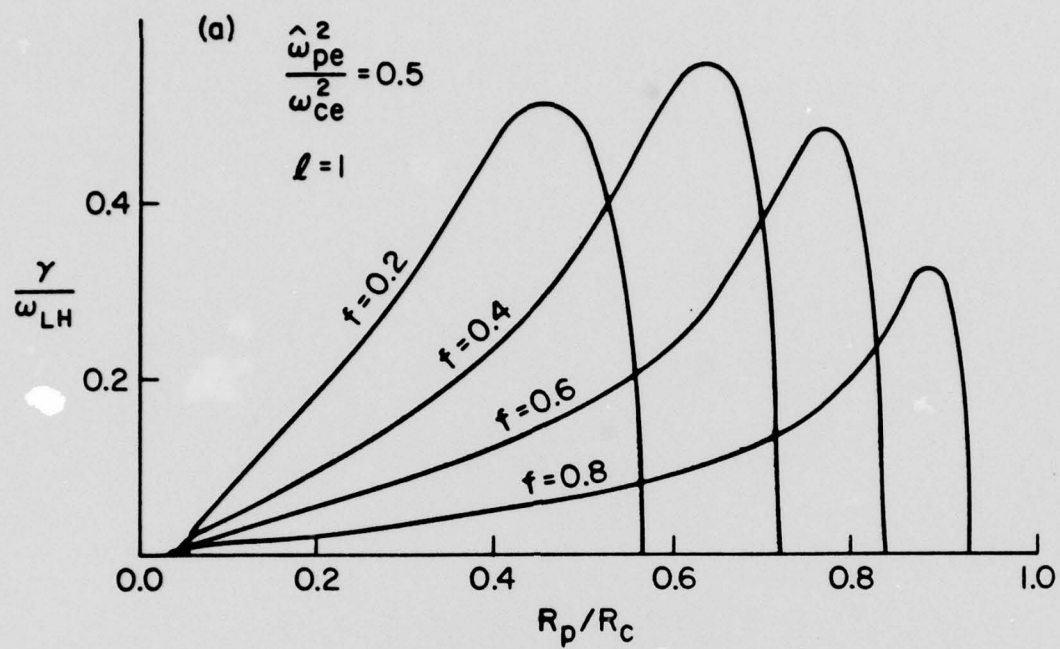


Fig. 14